RESEARCH ARTICLE

Provenance differentiation and earth surface process of the Mu Us sandy land constrained by detrital zircon U–Pb dating

Mengying He[1,2,3,4*] , Wanying Zhang[1,5], Bin Wang[6*] and Hongbo Zheng[7,8]

Abstract

Understanding the provenance and sediment surface processes of the Mu Us sandy land (MU) is critical for comprehending aeolian deposits and dust transportation in inland Asia and the Chinese Loess Plateau (CLP). In this study, we analyzed the detrital zircon U–Pb ages in the sediments of the MU, together with the previously collected data from sediments in the Hobq desert and CLP. Our findings demonstrate that there is spatial heterogeneity in the sediment characteristics of the MU and Hobq regions, with noticeable differences between northeastern and southwestern areas. In addition, the northeastern part of the CLP displays significant dissimilarities from other regions of the CLP. The NE MU, Eastern Hobq, and NE CLP inherit the main characteristics of basement rocks from the Western North China Craton, with prominent age ranges of 1600–2200 Ma and 2200–2800 Ma, indicating that this region is likely more controlled by in-situ weathering and recycling. In contrast, the SW MU, West-Middle Hobq and most parts of CLP show multiple sources, with a higher proportion of 200–350 Ma and 350–600 Ma, reflecting that the aeolian deposits in this area may be associated with more frequent earth surface processes such as sand-driving winds and fluvial transport. Although all three regions are situated within the square bend of the Yellow River and under the prevailing winds direction, sediments in the first two areas appear to have a more mixed contribution of both local and distal sources. In contrast, deposits in the CLP region were primarily sourced from the northeast Tibetan Plateau via the upper Yellow River. This indicates a variation in dust sources from north to south and suggests that the MU is part of the same sedimentary system as the CLP, rather than its direct source.

Keywords Mu Us sandy land, Chinese Loess Plateau, Provenance study, Detrital zircon U–Pb dating

*Correspondence:
Mengying He
conniehe@njnu.edu.cn
Bin Wang
bin.wang@snnu.edu.cn
[1] School of Geography Science, Nanjing Normal University, Nanjing 210023, China
[2] Jiangsu Open Laboratory of Major Scientific Instrument and Equipment, Nanjing Normal University, Nanjing 210023, China
[3] Jiangsu Center for Collaborative Innovation in Geographical Information Resource Development and Application, Nanjing 210023, China
[4] International Research Center of Big Data for Sustainable Development Goals, Beijing 100094, China
[5] College of Urban and Environmental Sciences, Peking University, Beijing 100871, China
[6] School of Geography and Tourism, Shaanxi Normal University, Xi'an 710119, China
[7] Research Center for Earth System Science, Yunnan University, Kunming 650091, China
[8] CAS Center for Excellence in Tibetan Plateau Earth Sciences, Beijing 100101, China

1 Introduction

Vast arid areas of Gobi and deserts have emerged in Asian inland under the global climate cooling in the Cenozoic, which turned into the essential dust archive from all over the world (Zachos et al. 2001; Muhs 2013). During the late Cenozoic, the thick and continuous aeolian dust deposits developed on the Chinese Loess Plateau (CLP), recording the interrelated history within the earth systems (Liu 1985; Liu and Ding 1998; Ding et al. 1998; An et al. 2001; Guo et al. 2002). The evolution of the modern Asian monsoon and inland deserts has been a key focus in the field of earth science (Guo et al. 2002; Chen et al. 2007; Sun 2002; Sun et al. 2013, 2018, 2020). However, during these decades, the exact provenance of the Asian dust deposits, especially on the CLP, is still under debate. Although many studies have suggested the proximal desert areas, under the influence of prevailing winds, are the main origin of dust on the CLP (Sun 2002; Yang and Ding 2008; Lu et al. 2011), it remains uncertain whether the western versus northwestern desert sources, influenced by the westerlies, or the East Asian winter monsoon (EAWM), respectively, or the impact of piedmont alluvial fans and river drainage, contribute to dust generation (Honda et al. 2004; Chen et al. 2007; Pullen et al. 2011; Stevens et al. 2010, 2013; Nie et al. 2015; Zhang et al. 2016, 2022).

The Mu Us sandy land (MU), located in the transition zone between the Gobi Desert and the Chinese Loess Plateau (CLP) in northern China, is particularly sensitive to the changes in climatic environment and earth surface processes (Fig. 1). The CLP's provenance is better understood by comprehending the MU. According to previous studies on the origin of MU sediments, they are believed to have originated from nearby areas and have undergone recycling from basement sandstones (Zhu et al. 1980; Sun 2000), and these sediments are an important source of CLP deposits, as recognized by Yang and Ding (2008). It has been recently discovered that the sediments in the MU exhibit differences in their composition depending on their location (Shu et al. 2017; Liu and Yang 2018; Wang et al. 2019; Bird et al. 2020; Chen et al. 2021). However, the exact extent and location of these variations are still unclear. According to studies given by Rao et al. (2011) and Ding et al. (2021), the sediments in the MU vary based on the size of the grains. Coarse-grained sand is likely derived from underlying sandstone while fine-grained sand is extensively mixed through long-distance aeolian and fluvial transport. The studies, conducted by Stevens et al. (2013) and Nie et al. (2015), utilized a combination of zircon U–Pb age pattern and heavy mineral analysis to investigate the contribution of proximal deserts and rivers in transporting dust to the Loess Plateau. They suggested that the Yellow River and its associated systems are responsible for carrying large quantities of sediments from northern Tibet to the western Mu Us desert and the CLP. However, these studies did not consider the inputs and contribution mixing from multiple sources of aeolian deposits.

Zircon grains can preserve the signal of crystallization age from source regions because of their high resistance to weathering and thermal alteration, and to alteration by the surface processes of deposition and transport (Griffin et al. 2004; Condie et al. 2005). Thus, detrital zircon U–Pb dating is widely used in sediment provenance studies, river evolution and basin research (He et al. 2014, 2021; Iizuka et al. 2010; Wang et al. 2022). In this study, we utilized detrital zircon U–Pb dating technique to date the surface sediments found in the MU. Additionally, we compared our findings with the published data of the Hobq desert in the north and CLP in the south, and evaluated them against all the potential sources that were considered in previous studies. The objectives of this study are: (1) to make a systematic provenance analysis for the MU sediments, as well as the precise range of sediment changes; (2) to quantify the relative contributions of potential sources to the surface sediments in the MU, Hobq Desert and CLP; and (3) to reveal the surface processes and relationships between these aeolian deposits.

2 Regional setting

The MU (37° 30′-39° 22.5′ N, 107° 20′–111° 30′ E), situated in the Ordos Basin, the Western North China Craton (NCC), is a steppe sandy land covered by sand dunes, loess deposits and grassland. The elevation of the MU ranges from ∼1200 to 1600 m a.s.L., and the altitude gradually decreases from northwest to southeast (Wang et al. 2019). The Yellow River acts roughly as the east and west boundary of the MU (Fig. 1), nearly covering an area of 4×10^4 km². The Mesozoic sandstones in the MU were altered by diluvial and alluvial processes during Paleocene to early Quaternary period and subsequently underwent aeolian erosion from the late Quaternary to the present day (Yang 2007). The sediment particle size in the MU gradually decreases from the northwest to the southeast (Shu et al. 2017), while the magnetic susceptibility presents a contrasting pattern (Cao et al. 2003). Currently, the area is predominantly comprised of Quaternary and modern deposits, with loosely cemented and highly weathered fuchsia Cretaceous sandstone cropping out in the north and west, and occasional exposures of grey-green Jurassic sandstone in the southeast (Fig. 2). To the north of the MU lies the Hobq Desert, while the CLP borders it to the south, which all lie within the square bend of the Yellow River. The Badain Jaran and the Tengger Desert lie to the northwest of the MU, and the Mongolian Gobi and Hunshandake sandy land locate in
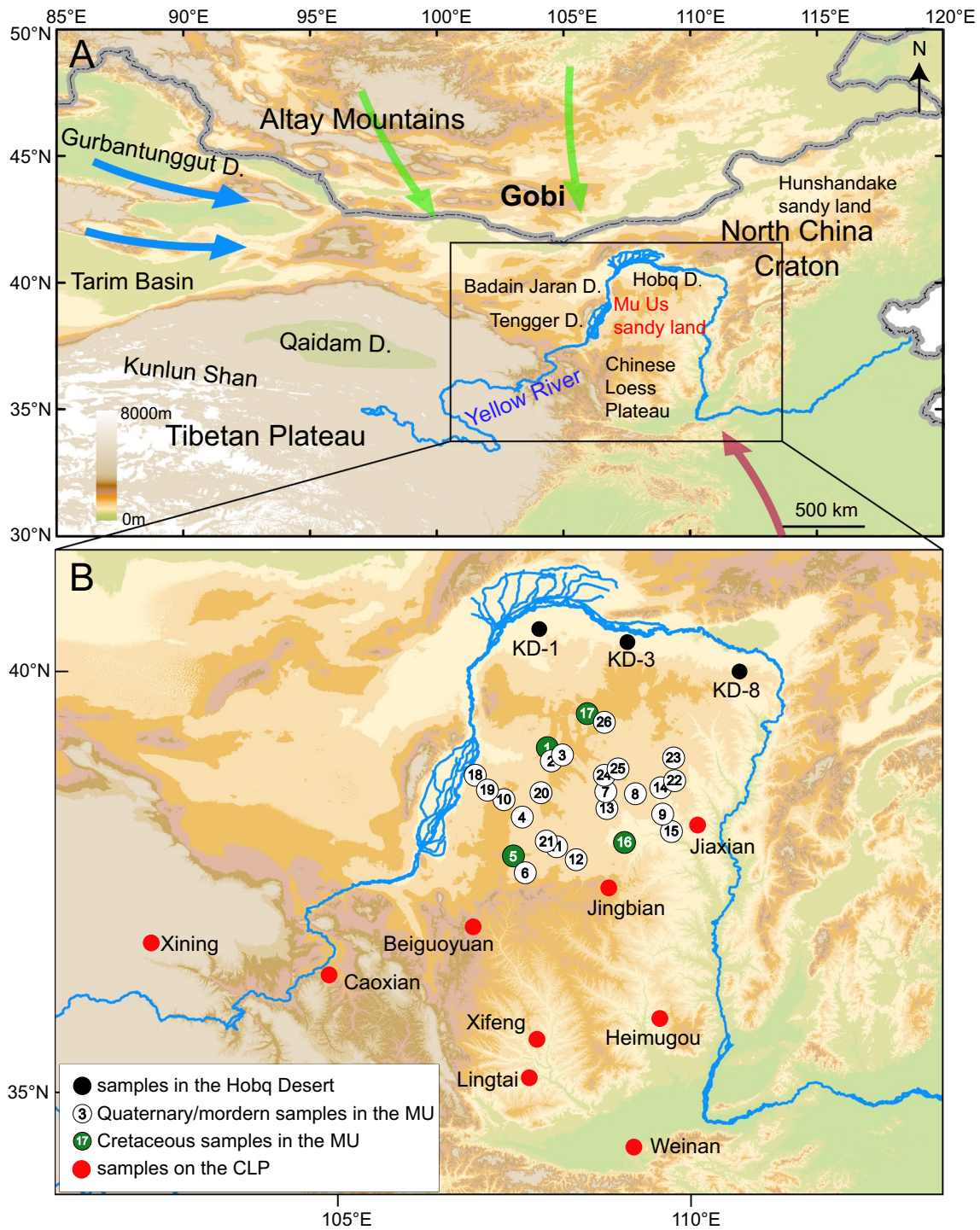
He *et al. Progress in Earth and Planetary Science* (2023) 10:63

Page 3 of 14

Fig. 1 **A** Topographic map of the study area and potential sources surrounding the Mu Us sandy land, modified from Stevens et al. (2013). Arrows show approximate directions of prevailing winds: blue-westerlies; green-East Asian winter monsoon; red-East Asian summer monsoon. **B** Sample locations in the Hobq deserts, Mu Us sandy land and Chinese Loess Plateau, including the samples in this study and previous studies (Table 1)

the further north (Fig. 1). The NE Tibetan Plateau in the southwest and the Tarim Basin further west of the MU are all considered as the potential sources of the CLP in

previous studies (Bird et al. 2015, 2020; Li et al. 2010; Che and Li 2013; Stevens et al. 2013; Nie et al. 2015; Zhang et al. 2016, 2022).
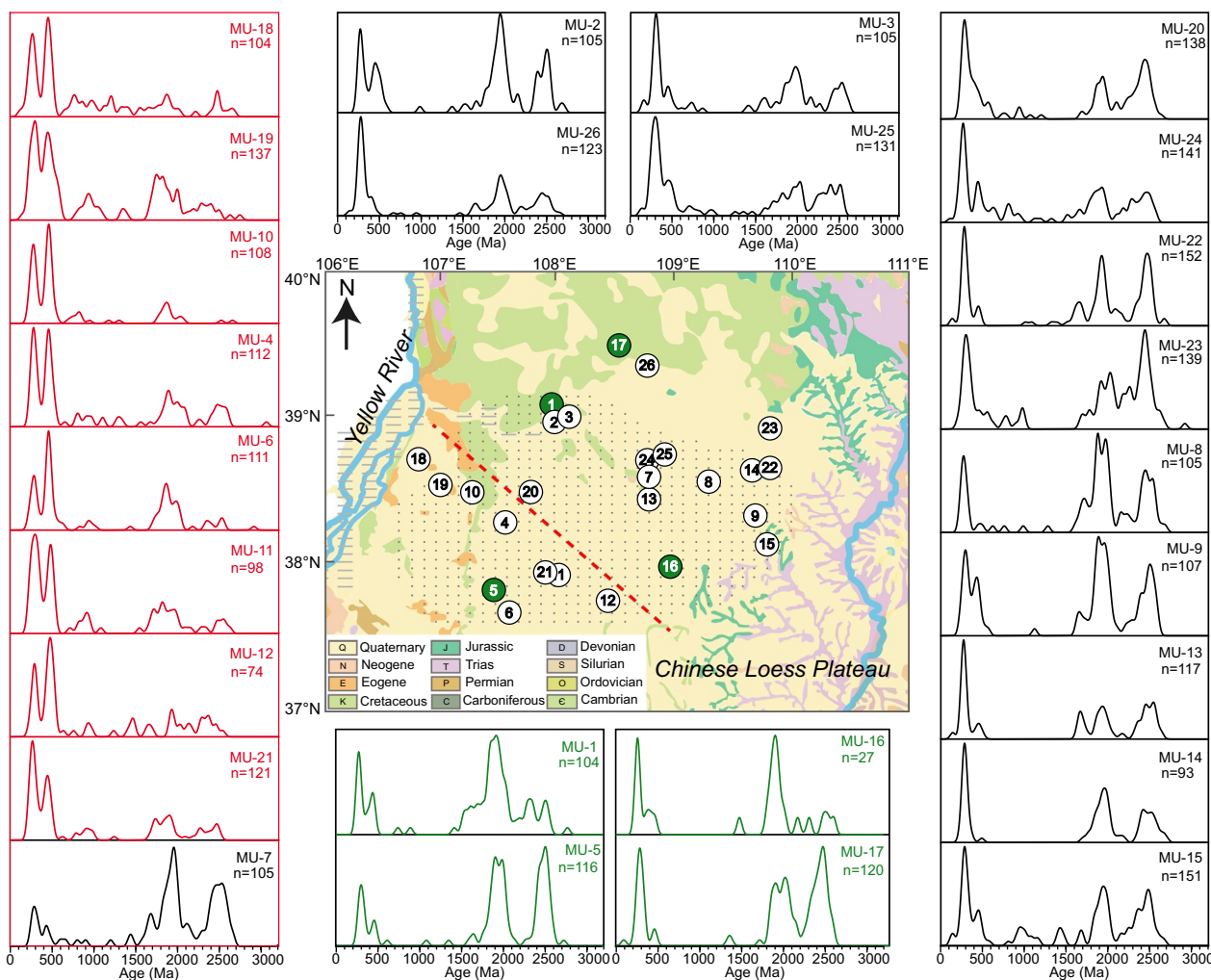
Fig. 2 Zircon U–Pb age spectra for sediments on the lithological map of the Mu Us sandy land (modified from the geological map of China, 1:2,500,000). The Cretaceous samples are marked with green dots and green lines. The red and black curve represent the SW MU part and the NE MU, respectively. The red dashed line represents two parts of the MU based on the zircon U–Pb ages

3 Samples and methods

A total of nine samples for surface sediments distributed throughout the MU were analyzed in this study, including two Cretaceous sandstone samples and seven surface Quaternary/modern sand samples. Sampling sites were chosen away from towns and roads, avoiding human pollutions. Each sample weighted 2–3 kg. We also collected samples' raw data of zircon U–Pb ages of the MU, Hobq Desert the CLP from previous studies in order to provide a comprehensive analysis of potential differential sources of sediments in this region. The sample distribution is depicted in Fig. 1B, and further details on each sample can be found in Table 1.

Zircon grains were extracted from sediment samples under the standard procedures of heavy liquids and magnetic separating. Most of the zircons were predominantly 100–200 μm grain size. 200–300 grains were randomly selected from each sample and were attached to the adhesive tape under the binocular microscope. After solidification with a mixture of epoxy resin and coagulant, we polished the resin pedestal until the grains maximum cross section appeared, then photograph zircons under the polarizing microscope before analysis.

The U–Pb dating was performed on the Laser ablation-inductively coupled plasma mass spectrometer (LA-ICP-MS) system at the School of Geographical Sciences, Nanjing Normal University, using a Photon Machine 193 nm laser ablation system coupled with an Ailgent 7700×quadrupole plasma mass spectrometer. The laser beam was 25–35 μm in diameter and 8 Hz in repetition rate. The international standard sample 91,500 (1062±4 Ma, Wiedenbeck et al. 1995) or GJ-1

Table 1 Sampling information on zircons from the Mu Us Sandy Land, Hobq desert and Chinese Loess Plateau

No	Sample ID	Longitude (°E)	Latitude (°N)	Data source
MU-1	160703-13	107.93	39.13	This study
MU-2	160704-1	107.95	39.03	
MU-3	160703-12	108.09	39.04	
MU-4	160704-4	107.53	38.3	
MU-5	160704-9	107.41	37.85	
MU-6	160704-10	107.53	37.67	
MU-7	160703-10	108.77	38.61	
MU-8	160703-3	109.3	38.58	
MU-9	160703-1	109.7	38.34	
MU-10	MD9	107.23	38.49	Stevens et al. (2013)
MU-11	MD10	107.99	37.92	
MU-12	MD4	108.49	37.71	
MU-13	MD2	108.76	38.48	
MU-14	MD7	109.66	38.65	
MU-15	MD1	109.79	38.14	
MU-16	MD3	108.49	37.71	
MU-17	MD5	108.82	37.99	
MU-18	MU51	106.9	38.7	Zhang et al. (2016)
MU-19	MU50	107.1	38.5	
MU-20	MU35	107.8	38.4	
MU-21	MU39	108	37.9	
MU-22	MU32	38.6	109.9	
MU-23	MU36	38.9	110	
MU-24	MU40	39.4	109	
MU-25	MU24	38.7	109	
MU-26	MU43	38.6	108.9	
Hobq Desert	Western	40.76	107.89	Zou (2017)
	Middle	40.38	109.23	
	Eastern	40.26	110.79	
Chinese Loess Plateau	Beiguoyuan	37.49	108.9	Bird et al. (2015)
	Jingbian	36.62	107.29	
	Lingtai	35.07	107.65	
	Weinan	34.35	109.51	Xiao et al. (2012)
	Xining	36.71	101.83	
	Caoxian	36.35	104.62	Che and Li (2013)
	Xifeng	35.77	107.77	
	Jiaxian	38.27	110.09	Zhang et al. (2021)
	Heimugou	35.72	109.61	Pullen et al. (2011)

(608.5 ± 0.4 Ma, Jackson et al. 2004) acted as the external standard while the "QingHu" sample (159.5 ± 0.2 Ma, Li et al. 2013) acted as the internal standard, to correct instrumental mass bias and ensure the reliability of the experimental data. To meet the statistical requirements for error reduction (Vermeesch 2004), we chose 168 grains in each randomly for in-situ laser ablation microanalysis. The argon gas works as carrier gas with the advantages of eliminating the elemental fractionation of Pb, Th and U. Experimental data were processed with the Igor Pro-Iolite program, $^{206}Pb/^{238}U$ ages were adopted for the grains younger than 1000 Ma, and $^{207}Pb/^{206}Pb$ ages for grains older than 1000 Ma (Griffin et al. 2004). The grains with discordance exceeding 10% among the ages of $^{206}Pb/^{238}U$, $^{207}Pb/^{235}U$ and $^{207}Pb/^{206}U$ were rejected. The Kernel Density Estimation (KDE) using bandwidth of 30

He *et al. Progress in Earth and Planetary Science*   (2023) 10:63

Page 6 of 14

Myr and non-metric multidimensional scaling (MDS) plots in the MATLAB-based software of DZmds were used to distinguish the relationship among detrital zircon datum of samples (Saylor et al. 2018). In order to quantify the relative contribution of these potential sources, we further adopted the DZ-Mix model presented by Sundell and Saylor (2017), using a MATLAB-based software for detrital zircon U–Pb inverse Monte Carlo mixture modeling. The DZ-mix model was made using three statistic methods: Cross-correlation, KS and Kuiper with 10,000 trials. Raw zircon U–Pb age data are available in Additional file 1: Table S1.

4 Results

We adopt the KDE to create age spectra visualizations for the zircon samples (Vermeesch 2012) (Fig. 2). The age spectra of sediments in the MU show multiple age peaks, which could be divided into five main age groups of 200–350 Ma, 350–600 Ma, 600–1600 Ma, 1600–2200 Ma, and 2200–2800 Ma. Zircon ages younger than 200 Ma and older than 2800 Ma appear very rarely and show little distinct distribution patterns. After combining 17 samples from Stevens et al. (2013) and Zhang et al. (2016), we classify the total 26 detrital zircon samples from the MU into two groups for further analysis: the Cretaceous samples and Quaternary/modern samples.

Samples of the MU1, MU5, MU16 and MU-17 are representative of the Cretaceous samples in the MU (Fig. 2), displaying prominent age peaks of 200–350 Ma, 1600–2200 Ma, 2200–2800 Ma, and a side peak of 350–600 Ma. The zircon U–Pb age spectra of other modern samples in the MU show distinct spatial differences, which could be roughly divided into two regions: the northeast and southwest parts (Fig. 2). Most samples belong to the northeastern (NE) MU parts, which resemble the Cretaceous basement samples, with a higher content of 200–350 Ma, 1600–2200 Ma and 2200–2800 Ma zircons, while those from the southwestern (SW) MU exhibit a higher percentage of both the 200–350 Ma and 350–600 Ma zircons, with a notably lower content of older zircons.

To further confirm the division observed in the U–Pb age spectra, we present two-dimensional MDS diagram that illustrates the physical distances between samples (Fig. 3). The similarities are represented by solid lines and dotted lines, which refer to primary and secondary correlations, respectively (Borg and Groenen 2003). The MU samples are clearly divided into two groups (Fig. 3A): the NE and Cretaceous MU, and the SW MU, which are consistent with the U–Pb age spectra results. Similarly, the spatial characteristics of sediment in the Hobq Desert and CLP also differ, with the eastern Hobq, northeastern CLP and NE MU exhibiting more similarity, and the

middle and western Hobq and most samples on the CLP being more alike the SW MU (Fig. 3B). Although previous studies have suggested that dust deposits on the CLP exhibit spatial heterogeneity (Xie et al. 2012; Xiao et al. 2012; Bird et al. 2015; Ma et al. 2019; Zhang et al. 2021; Xiong et al. 2023), compared with the MU, the zircon age patterns of most loess samples do not show clear differences in Fig. 3B, as they all overlap with the region where the SW MU is found. It is not surprising that the sample of Jiaxian, which is located in the northeastern CLP displays similar characteristic with the NE MU, since they all lie within the western North China Craton. Recent work has proposed that the detrital zircon U–Pb dating requires a large number of grains (n > 300) for each sample to avoid the sample size effect on the provenance analysis (Licht et al. 2016; Zhang et al. 2016; Chen et al. 2022). Thus, we combined samples with similar zircon characteristics to achieve enough grain numbers for provenance identification. According to the clustering, we were able to categorize them into the following groups: the NE MU, SW MU, Cretaceous MU, East Hobq, West-Middle Hobq, NE CLP and CLP.

5 Discussion

5.1 Provenance identification from zircon U–Pb ages

Since the sediments in the MU display five major age groups, it is likely that the area has multiple sources rather than a single source. The zircon U–Pb ages of these sediments were mainly controlled by the regional geological units and major magmatic events nearby. Previous studies on dust sources in this region have yielded inconsistent results, primarily due to disparities in the selection of potential sources as end-members (Xiao et al. 2012; Stevens et al. 2013; Zhang et al. 2016; Xiong et al. 2023). In this study, we compiled the published data regarding detrital zircon U–Pb ages from all the potential sources of the MU and CLP, including the NE Tibetan Plateau (the Qaidam, Songpan-Ganzi, and its piedmont), the northwest deserts (the Badain Jaran Desert and the Tengger Desert, which are mainly derived from the Altai Mountains), the north gobi, the western NCC, and the Taklimakan desert in the Tarim Basin, to comprehensively discuss the source contribution to the MU sediments (Fig. 4).

The cumulative distribution curves of the dust samples and the potential sources reveal a clear classification (Fig. 4A), with two distinct curve features. The Cretaceous MU, NE MU, NE CLP, Western NCC and East Hobq display a similar curve pattern to each other, while the other sections are more closely related, indicating the different zircon age compositions of these two groups.

The analysis of the clustered samples also reveals visible variations in the zircon KDE plots (Fig. 4B). The
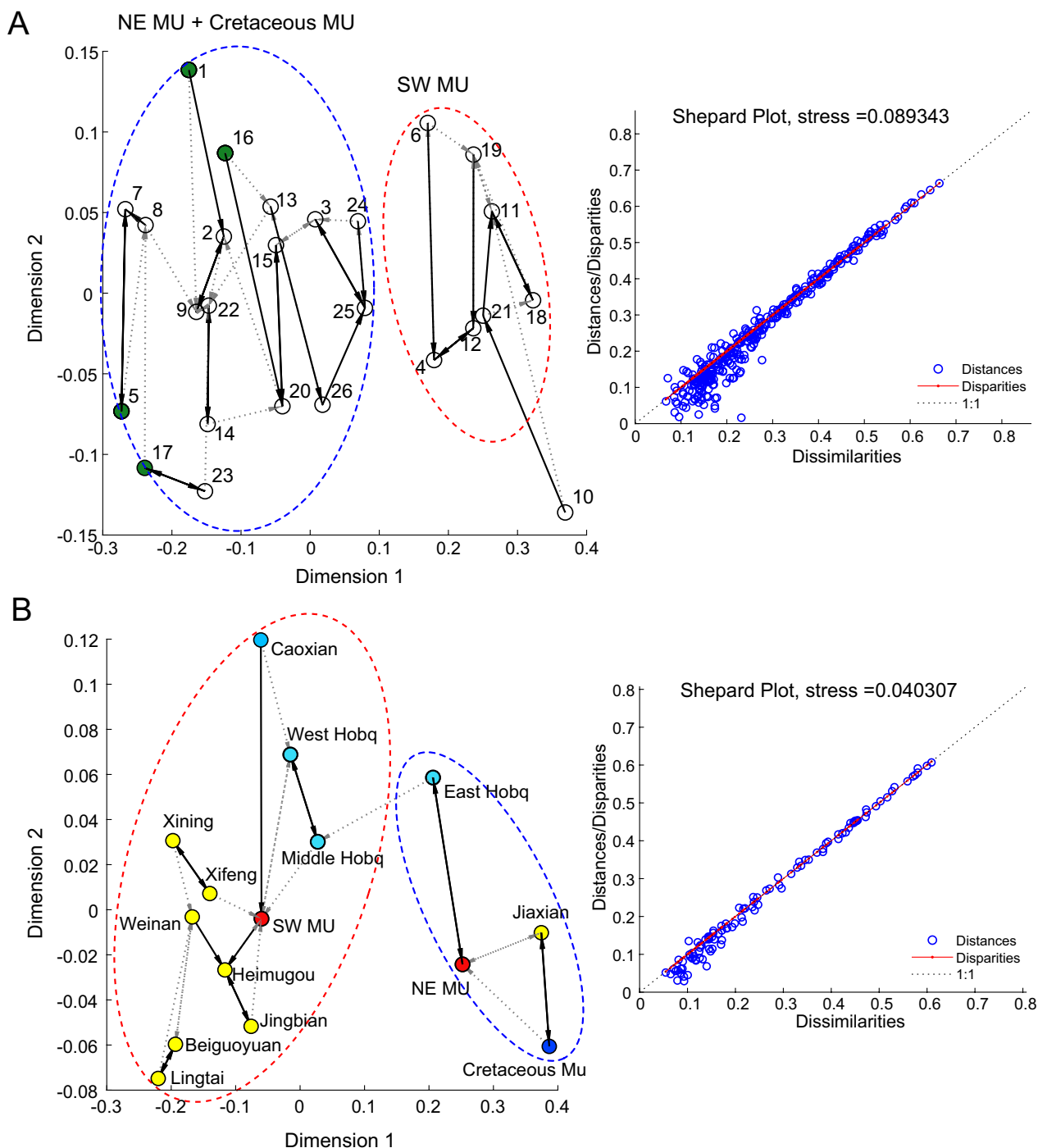
Fig. 3 A Two-dimensional multidimensional scaling (MDS) diagram and Shepard plot of zircon U–Pb age spectra for the sediments in the Mu Us sandy land. **B** The MDS and Shepard plots of zircon U–Pb age spectra for samples in the Hobq desert, Mu Us sandy land and the CLP

Neoarchean and Paleo-proterozoic age groups, spanning from 2200–2800 Ma and 1600–2200 Ma, respectively, with an age peak around 2.5 Ga and 1.8 Ga, largely correspond to the accelerated global crustal growth period and the ages of the Lüliangian Orogeny (Condie et al.

2009; Rino et al. 2004). It is possible that the NCC basement formed due to mantle plume activities (Wan et al. 2006; Zhai and Peng 2007; Zhao and Zhai 2013), and the time of complete cratonization occurred approximately 2.45 Ga (Kusky and Li 2003; Kusky et al. 2016; Zhai 2014,
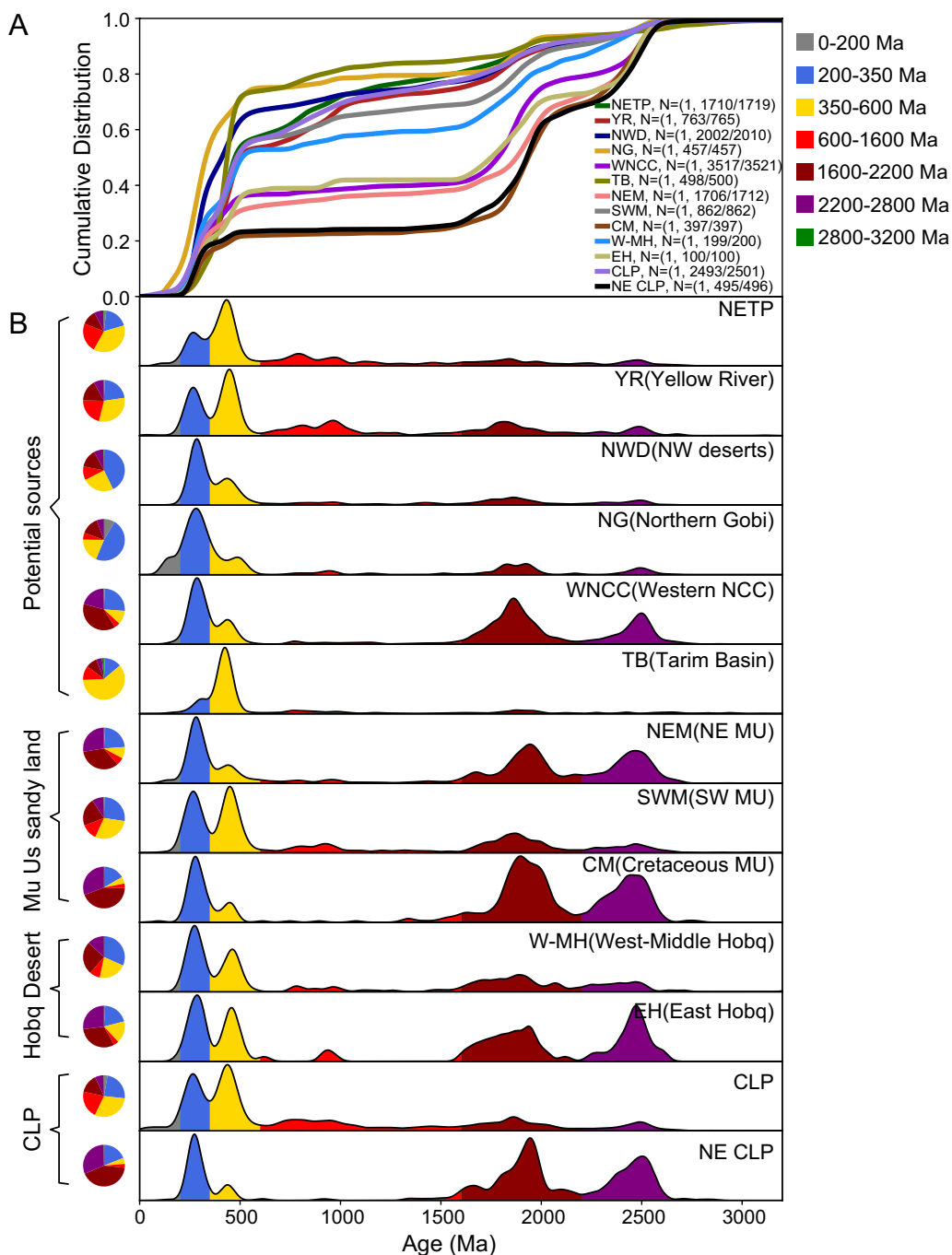
Fig. 4 Cumulative distribution plot (**A**), zircon U–Pb age spectra and pie charts (**B**) from sediments in the Mu Us sandy land, Hobq desert, CLP, and potential sources. Data for the Western North China Craton were obtained from Darby and Gehrels (2006), Li et al. (2010), Hu et al. (2013), Qu et al. (2020), Licht et al. (2016), Chen et al. (2021). Data for the Tarim Basin were obtained from Xie et al. (2007) and Yang et al. (2013). Data for the Northeastern Tibetan Plateau were obtained from Gehrels et al. (2003a), Pullen et al. (2011), Licht et al. (2016), Zhang et al. (2016) and Nie et al. (2015). Data for the northern Gobi were obtained from Zou (2017), Pullen et al. (2011) and Xie et al. (2007). Data for the NW deserts were obtained from Nie et al. (2015), Stevens et al. (2010), Licht et al. (2016) and Zhang et al. (2016); Data for the NE CLP was obtained from Zhang et al. (2021)

2019). The NCC underwent late phases of accretion during the age around 1.8 Ga, including the merging of basement and uplifting and denudation, followed by series of magmatic events, related to the breakup of the Columbia supercontinent in 1.6–1.8 Ga in the early Meso-proterozoic (Pan et al. 2016; Enkelmann et al. 2007). Thus, the percentage of old zircons at 2800–2200 Ma and 2200–1600 Ma are notably higher in the Western NCC (38% and 21%, respectively) compared to other potential sources (Fig. 4B). Among the aeolian deposits, the Cretaceous MU (44% and 30%), NE MU (34% and 27%), NE CLP (42% and 31%) and East Hobq (31% and 27%) all contain a considerable number of old zircons (Table 2), indicating a more contribution from the Western NCC to these regions.

The age group of 350–600 Ma corresponds to the events that associated with the subduction and collision of the Qilian Mountains and the west Qinling Orogenic Belt (Xu et al. 2008; Yong et al. 2008; Wu et al. 2012; Yang et al. 2015). Zircons of 600–1600 Ma may have originated from the Qaidam Basin (Gehrels et al. 2003b; Pullen et al. 2011), although few plutons dating within this age range have been found in other potential source areas. The NETP and Yellow River both display high concentrations of zircons in these two age groups, with percentages of 38% and 23%, and 31% and 21%, respectively. The same pattern is also observed in the SW MU, West-Middle Hobq and CLP deposits. Conversely, the Tarim Basin exhibits an exceptionally high percentage of the 350–600 Ma zircons, indicating its proper contribution to the dust deposition in this area.

The age group of 200–350 Ma is generally prominent in all the samples from the MU, Hobq Desert, and all the CLP. Previous research suggests that the metamorphic basement of the NW deserts, such as Tengger and Badain Jaran Desert, which are exposed to the EAWM that blows toward the MU, primarily originated from several Early Permian granite intrusions (Zhang et al. 2016). Xu et al. (2008) also indicate that the East Kunlun Shan, which developed as a volcanic arc during 240–270 Ma, could be a significant source of sediment supply to the MU through the prevailing winds. Therefore, all the potential sources have the possibility to supply materials to the study area (Table 2). In contrast, the Tarim Basin shows a lower percentage of this particular zircon age group, indicating its relatively lower contribution under the westerly wind.

The younger zircons of the 0–200 Ma age group are present in low concentrations in all the samples and potential sources, except for the NETP and the Gobi. However, it is difficult to identify the sediment sources based solely on this age group.

The 3-D MDS plot clearly shows the relationship between dust deposits and the potential sources (Fig. 5). The NE MU, Cretaceous MU, NE CLP and East Hobq show significant association with the Western NCC, indicating that sediments in these areas mainly originate from the underlying bedrock of the local sources. In contrast, the SW MU, Middle-West Hobq, and the CLP are closely related to the NETP and the Yellow River, while the NW deserts and Gobi show the second association. The Tarim Basin lies relatively far from the SW MU, indicating their limited contributions to the dust deposition in this area.

The DZ mix model made by the Cross-correlation of the KDEs were chosen to calculate the proportion of

Table 2 The proportion of each age group in surface samples from the Mu Us Desert and potential sources

| Sample ID	0–200 Ma (%)	200–350 Ma (%)	350–600 Ma (%)	600–1600 Ma (%)	1600–2200 Ma (%)	2200–2800 Ma (%)	2800–3200 Ma (%)
Crataceous MU	0	16	5	4	44	30	0
NE MU	1	23	9	6	34	27	0
SW MU	1	27	29	12	22	9	0
CLP	3	24	30	21	15	7	0
NE CLP	0	19	5	3	42	31	0
East Hobq	1	20	17	4	31	27	0
Middle-West Hobq	0	31	21	11	25	13	0
NETP	2	19	38	23	12	7	0
Yellow River	1	22	31	21	17	8	0
NW deserts	0	43	25	11	14	7	0
Gobi	2	48	29	11	9	1	0
Western NCC	1	25	11	4	38	21	0
Tarim Basin	1	13	60	11	9	4	2
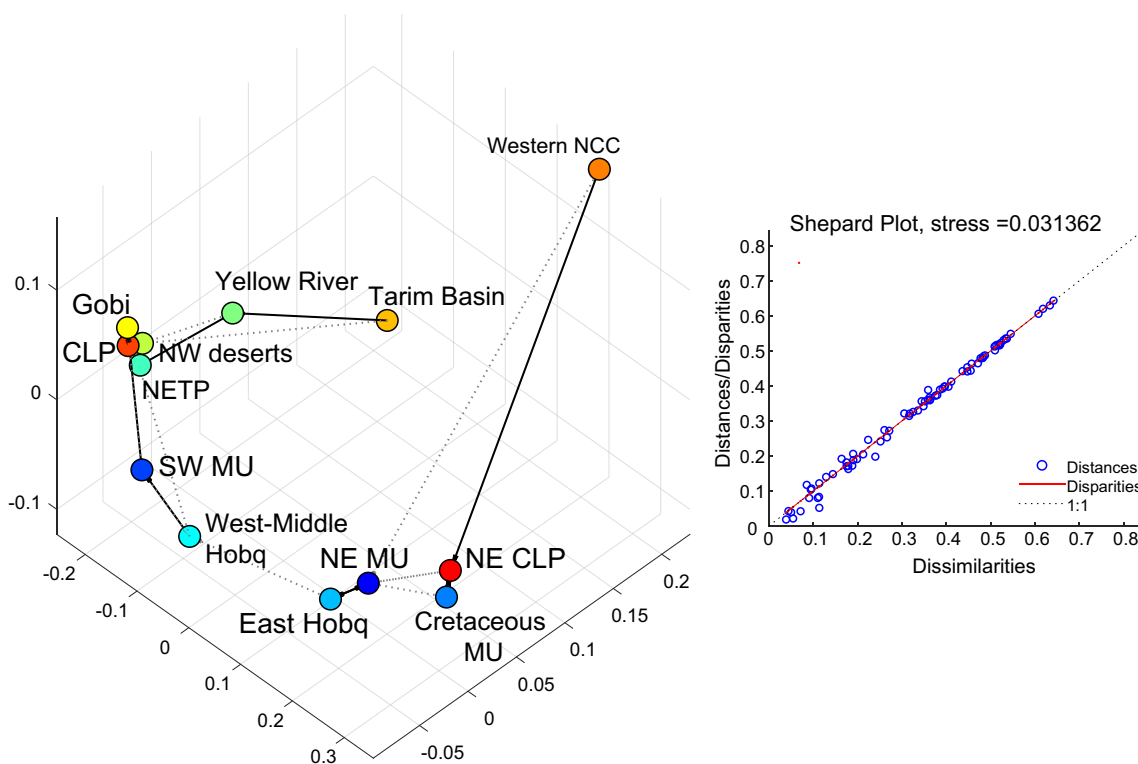
Fig. 5 Three-dimensional multidimensional scaling (MDS) diagram and Shepard plot of zircon U–Pb age spectra for the sediments of eolian deposits of the Mu Us sandy land, Hobq and Chinese Loess Plateau, and the potential sources
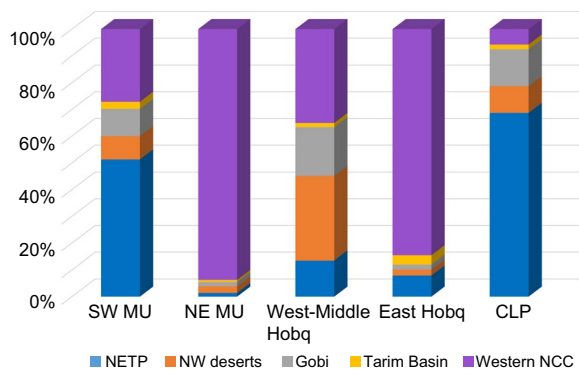

Fig. 6 The relative contribution and cumulative probability of each potential source to the Mu Us sandy land, Hobq desert and CLP, respectively

Conversely, the dust deposition in the SW MU, West-Middle Hobq and CLP show notable differences in the contributions, although they have similar zircon age distributions. Sediments in the SW MU mainly originated from the NETP, followed by the Western NCC, Gobi and NW deserts, with only 3% coming from the Tarim Basin. In contrast, the NW deserts and the Western NCC are the primary contributors to the West-Middle Hobq, with relatively few materials from the Gobi and NETP. Regarding the CLP, the NETP contributes approximately 69% of the sediments, while the NW deserts and Gobi contribute approximately 10% each, and the Western NCC accounts for 6% of the deposited dust (Table 3). All the samples show little contribution from the Tarim Basin, indicating that the far-off desert has little significance for this area.

5.2 Surface processes of sediments of the aeolian deposits
As demonstrated from the above analysis, there are significant spatial differences in the material sources of the Mu Us sandy land, which can be classified into the NE and SW regions, consistent with previous research (Stevens et al. 2013; Nie et al. 2015; Ding et al. 2021). The MU shows a clear segregation, with most parts belonging to

potential sources because its higher Cross-correlation value and lower standard deviation than the other two methods (Fig. 6, Table 3). It is not surprising that the contribution histogram based on the DZ-Mix model demonstrates similar pattern of the NE MU and East Hobq, which are primarily supplied by the Western NCC, with minor contributions from the NETP and other sources.

Table 3 Proportions of potential sources contributing at successive ages

Sample ID	SW MU (%)	NE MU (%)	West-Middle Hobq (%)	East Hobq (%)	Chinese Loess Plateau (%)
NE Tibetan Plateau	51	1	13	8	69
NE deserts	9	2	32	2	10
Northern Gobi	10	2	18	2	14
Tarim Basin	3	1	2	3	2
Western North China Craton	27	94	35	85	6

the NE region (Fig. 2), mainly comprising proximal materials from the Western NCC and exposed Cretaceous rocks. Only a small part of the MU adjacent to the northern CLP belongs to the SW MU part. The features of the Eastern Hobq Desert in the north correspond with those of the NE MU, and the West-Middle Hobq and CLP exhibit a similar zircon age distribution to the SW MU, characterized by a multi-source feature.

Previous studies based on several proxies including detrital zircon ages and heavy minerals (Stevens et al. 2013; Nie et al. 2015; Yang et al. 2022; Zhang et al. 2022), carbonate minerals (Meng et al. 2019) and geochemistry methods (Chen et al. 2007; Li et al. 2011, 2018) have attributed prevailing winds as the primary cause of the aeolian deposition, stating that the dust material mainly comes from the Tarim Basin and the NW deserts and Gobi under the westerlies or the EAWM. Recent research suggests that the west MU and CLP predominantly consists of materials carried by the Yellow River from the NETP (Stevens et al. 2013; Nie et al. 2015; Zhang et al. 2022). In this study, we found that the sources of the aeolian deposition of the MU, Hobq and CLP varies among different locations, despite the fact they all are situated within the prevailing winds range and the square bend of the Yellow River. These three areas all display both local and distal sources, but from north to south, the contributions of the NW desert and Gobi are much greater than the Tarim Basin, indicating that the EAWM may be more important than the westerly wind on dust transportation to this area, which is also consistent with the southeast decreasing grain size in the MU (Rao et al. 2011; Ding et al. 2021). Coarse-grained materials are more easily obstructed by rivers, lakes, and other obstacles, whereas fine-grained material can continue to be transported (Wang et al. 2019). Therefore, the West-Middle Hobq and SW MU received more coarse-grained deposits from the NW desert and northern Gobi area under the EAWM, but the East Hobq and NE MU mainly deposited the local materials, resulting in the spatial differences in the Hobq desert and Mu Us sandy land. While fine-grained materials were transported further to the CLP, and exhibited similar dust compositions between the NE

CLP and NE MU. Additionally, most parts of the CLP have large influence from the floodplain deposits of the Yellow River under the wind-blow. Thus, it is suggested that both the prevailing winds and the fluvial fan (the Yellow River) may not have as much influence as originally believed. Neither factor independently determines the deposition of aeolian dust as previous studies have suggested. Instead, the sources of aeolian dust largely vary depending on factors such as sediment grain size, depositional locations, and even the sedimentary mass of the river floodplain.

Furthermore, our study also indicates that the majority of the dust deposits on the CLP originate from the NETP and are relatively uniform compared to those found in the Hobq and MU. There is little contribution from the Western NCC (except in the NE CLP), indicating that the MU is not the direct source region of the CLP, but both belong to the same sedimentary system controlled by the prevailing winds. However, it is still possible that fine-grained materials in the SW MU are blown into the CLP. Although our study highlights the importance of the Yellow River in contributing to the CLP, further investigation is required to verify the source changes under different climatic conditions, particularly when considering the characteristics of the Hobq and MU.

6 Conclusions
This study carried out the detrital zircon U–Pb dating of sediments in the Mu Us sandy land (MU), and combined the data from the aeolian deposit of the Chinese Loess Plateau (CLP) and Hobq Desert to illustrate sediment source variability. The sediments from the MU and Hobq Desert could obviously be divided into two distinct parts: the northeast and southwest, and the northeast CLP show distinct difference with other part of CLP. Sediments from the NE MU, NE CLP and East Hobq were mostly derived from the underlying basements of the Western North China Craton, experiencing more localized physical recycling. In contrast, although the SW MU, West-Middle Hobq and CLP are all situated within the prevailing winds range and in proximity to the Yellow River, sediments in the former

two regions display more mixture of local and distal sources, while most part of the CLP deposits were dominated by the NE Tibetan Plateau via the upper Yellow River. This indicates a variation in dust source from north to south. According to the correlation analysis, we hold the opinion that the materials brought by the prevailing winds (mainly the EAWM) are more coarse-grained sediments, while the fine grained materials on the CLP are more from the NETP via the Yellow River. Surface sediments in the NE MU have little affinity with the loess in the CLP in provenance. Instead, the SW MU can be regarded as a part of the same sedimentary system as the CLP, rather than the direct source region.

Abbreviations

MU	Mu Us sandy land
CLP	Chinese Loess Plateau
NE MU	Northeast Mu Us sandy land
SW MU	Southwest Mu Us sandy land
NETP	Northeast Tibetan Plateau
NCC	North China Craton
NW desert	Northwest desert
YR	Yellow river
KDE	Kernel density estimation
MDS	Multidimensional scaling
EAWM	East Asian winter monsoon

Supplementary Information

The online version contains supplementary material available at https://doi.org/10.1186/s40645-023-00596-6.

> **Additional file 1. Table S1.** Detrital zircon U-Pb ages of sediments in the Mu Us sandy land from this work.

Author contributions

ZHB and HMY conceived and designed the study. HMY and WB collaborated in the sampling collection. ZWY carried out the experimental study and obtained analytical data. HMY collaborated with the WB in the construction of manuscript. All authors read and approved the final manuscript.

Availability of data and materials

The dataset supporting the conclusions of this article is included within the article (and its additional files).

Declarations

Competing interests

The authors declare no competing interests.

References

An Z, Kutzbach JE, Prell WL, Porter SC (2001) Evolution of Asian monsoons and phased uplift of the Himalaya-Tibetan plateau since Late Miocene times. Nature 411:62–66

Bird A, Stevens T, Rittner M, Vermeesch P, Carter A, Andò S, Garzanti E, Lu H, Nie J, Lin Z, Zhang H, Xu Z (2015) Quaternary dust source variation across the Chinese Loess Plateau. Palaeogeogr Palaeoclimatol Palaeoecol 435:254–264

Bird A, Millar I, Rodenburg T, Stevens T, Rittner M, Vermeesch P, Lu H (2020) A constant Chinese Loess Plateau dust source since the late Miocene. Quaternary Sci Rev 227:106042

Borg I, Groenen P (2003) Modern multidimensional scaling: theory and applications. J Educ Meas 40(3):277–280

Cao HX, Zhang YX, Yue LP, Wang Y (2003) Characteristics of grain size composition Holocene deposits and its Paleoclimatic significance in Mu Us Sandy Land. Acta Sedimentol Sin 21(3):482–486

Che X, Li G (2013) Binary sources of loess on the Chinese Loess Plateau revealed by U-Pb ages of zircon. Quat Res 80(3):545–551

Chen J, Li G, Yang J, Rao W, Lu H, Balsam W, Sun Y, Ji J (2007) Nd and Sr isotopic characteristics of Chinese deserts: Implications for the provenances of Asian dust. Geochim Cosmochim Acta 71(15):3904–3914

Chen G, Dong Z, Li C, Shi W, Shao T, Nan W, Yang J (2021) Provenance of Aeolian sediments in the ordos deserts and its implication for weathering sedimentary processes. Front Earth Sci 9:711802

Chen X, Lyu K, Wang P, Huang X, Kong X (2022) A review of research progress on the analytical method of large-n detrital zircon U-Pb geochronology. Rock Miner Anal 41(6):920–934

Condie KC, Beyer E, Belousova E, Griffin WL, O'Reilly SY (2005) U-Pb isotopic ages and Hf isotopic composition of single zircons: the search for juvenile Precambrian continental crust. Precambrian Res 139(1–2):42–100

Condie KC, Belousova E, Griffin WL, Sircombe KN (2009) Granitoid events in space and time: constraints from igneous and detrital zircon age spectra. Gondwana Res 15(3–4):228–242

Darby BJ, Gehrels G (2006) Detrital zircon reference for the North China block. J Asian Earth Sci 26(6):637–648

Ding Z, Sun J, Liu T, Zhu R, Yang S, Guo B (1998) Wind-blown origin of the Pliocene red clay formation in the central Loess Plateau China. Earth Planet Sci Lett 161(1–4):135–143

Ding J, Wu Y, Tan L, Fu T, Du S, Wen Y, Li D (2021) Trace and rare earth element evidence for the provenances of aeolian sands in the Mu Us Desert NW China. Aeolian Res 50:100683

Enkelmann E, Weislogel A, Ratschbacher L, Eide E, Renno A, Wooden J (2007) How was the Triassic Songpan-Ganzi basin filled? A provenance study. Tectonics 26(4)

Gehrels GE, Yin A, Wang X (2003a) Detrital-zircon geochronology of the northeastern Tibetan plateau. Geol Soc Am Bull 115(7):881–896

Gehrels GE, Yin A, Wang X (2003b) Magmatic history of the northeastern Tibetan Plateau. J Geophys Res: Solid Earth 108(B9)

Griffin WL, Belousova EA, Shee SR, Pearson NJ, O'Reilly SY (2004) Archean crustal evolution in the northern Yilgarn Craton: U-Pb and Hf-isotope evidence from detrital zircons. Precambrian Res 131:231–282

Guo Z, Ruddiman WF, Hao Q, Wu H, Qiao Y, Zhu R, Peng S, Wei J, Yuan B, Liu T (2002) Onset of Asian desertification by 22 Myr ago inferred from loess deposits in China. Nature 416:159–163

He MY, Zheng HB, Bookhagen B, Clift PD (2014) Controls on erosion intensity in the Yangtze River basin tracked by U-Pb detrital zircon dating. Earth-Sci Rev 136:121–140

He MY, Zheng HB, Clift PD, Bian ZC, Yang Q, Zhang BH, Xia L (2021) Paleogene sedimentary records of the Paleo-Jinshajiang (Upper Yangtze) in the Jianchuan Basin Yunnan SW China China. Geochem Geophys Geosyst 22(6):e2020GC009500

Honda M, Yabuki S, Shimizu H (2004) Geochemical and isotopic studies of Aeolian sediments in China. Sedimentology 51:211–230

Hu J, Liu X, Li Z, Zhao Y, Zhang S, Liu X, Qu H, Chen H (2013) SHRIMP U-Pb zircon dating of the Ordos Basin basement and its tectonic significance. Chin Sci Bull 58(1):118–127

Iizuka T, Komiya T, Rino S, Maruyama S, Hirata T (2010) Detrital zircon evidence for Hf isotopic evolution of granitoid crust and continental growth. Geochim Cosmochim Acta 74(8):2450–2472

Jackson SE, Pearson NJ, Griffin WL, Belousova EA (2004) The application of laser ablation-inductively coupled plasma–mass spectrometry to in situ U-Pb zircon geochronology. Chem Geol 211:47–69

Kusky TM, Li J (2003) Paleoproterozoic tectonic evolution of the North China Craton. J Asian Earth Sci 22(4):383–397

Kusky TM, Polat A, Windley BF, Burke KC, Dewey JF, Kidd WSF, Maruyama S, Wang J, Deng H, Wang Z, Wang C, Fu D, Li X, Peng H (2016) Insights into the tectonic evolution of the North China Craton through comparative tectonic analysis: a record of outward growth of Precambrian continents. Earth-Sci Rev 162:387–432

Li H, He B, Xu Y, Huang X (2010) U-Pb and Hf isotope analyses of detrital zircons from Late Paleozoic sediments: insights into interactions of the North China Craton with surrounding plates. J Asian Earth Sci 39(5):335–346

Li GJ, Pettke T, Chen J (2011) Increasing Nd isotopic ratio of Asian dust indicates progressive uplift of the north Tibetan Plateau since the middle Miocene. Geology 39(3):199–202

Li XH, Tang GQ, Guo B, Gong B, Yang YH, Hou KJ, Hu ZC, Li QL, Liu Y, Li WX (2013) Qinghu zircon: a working reference for microbeam analysis of U-Pb age and Hf and O isotopes. Chin Sci Bull 58(20):1954–1961

Li L, Chen J, Chen Y, Hedding DW, Li T, Li LF, Liu XJ, Zeng FM, Wu WH, Zhao L, Li GJ (2018) Uranium isotopic constraints on the provenance of dust on the Chinese Loess Plateau. Geology 46(9):747–750

Licht A, Pullen A, Kapp P, Abell J, Giesler N (2016) Eolian cannibalism: reworked loess and fluvial sediment as the main sources of the Chinese Loess Plateau. GSA Bull 128(5/6):944–956

Liu T (1985) Loess and the environment. China Ocean, Beijing

Liu T, Ding Z (1998) Chinese loess and the paleomonsoon. Annu Rev Earth Planet Sci 26(1):111–145

Liu Q, Yang X (2018) Geochemical composition and provenance of aeolian sands in the Ordos Deserts northern China. Geomorphology 318:354–374

Lu H, Mason JA, Stevens T, Zhou Y, Yi S, Miao X (2011) Response of surface processes to climatic change in the dunefields and Loess Plateau of North China during the late Quaternary. Earth Surf Proc Land 36:1590–1603

Ma R, Zhang W, He M (2019) Spatial difference of provenance of the loess on Loess Plateau based on detrital zircon U-Pb age. Mar Geo Front 35(1):24–31

Meng XQ, Liu LW, Zhao W, He T, Chen J, Ji JF (2019) Distant Taklimakan Desert as an important source of Aeolian deposits on the Chinese Loess Plateau as evidenced by carbonate minerals. Geophys Res Lett 46(9):4854–4862

Muhs DR (2013) Geologic records of dust in the Quaternary. Aeolian Res 9:3–48

Nie J, Stevens T, Rittner M, Stockli D, Garzanti E, Limonta M, Bird A, Andò S, Vermeesch P, Saylor J, Lu H, Breecker D, Hu X, Liu S, Resentini A, Vezzoli G, Peng W, Carter A, Ji S, Pan B (2015) Loess plateau storage of northeastern Tibetan plateau-derived Yellow River sediment. Nat Commun 6:8511

Pan G, Lu S, Xiao Q, Zhang K, Yin F, Hao G, Luo M, Ren F, Yuan S (2016) Division of tectonic stages and tectonic evolution in China. Earth Sci Front 23(6):10–23

Pullen A, Kapp P, McCallister AT, Chang H, Gehrels GE, Garzione CN, Heermance RV, Ding L (2011) Qaidam Basin and northern Tibetan Plateau as dust sources for the Chinese Loess Plateau and paleoclimatic implications. Geology 39(11):1031–1034

Qu HJ, Han X, Chen S, Yang B, Du MY, Dong YY, Zhao C (2020) U-Pb dating of detrital zircon from the upper paleozoic clastic rocks and basin-mountain coupling of the northeastern Ordos Basin. Geotecton Metallog 44(3):501–513

Rao W, Tan H, Jiang S, Chen J (2011) Trace element and REE geochemistry of fine-and coarse-grained sands in the Ordos deserts and links with sediments in surrounding areas. Geochemistry 71(2):155–170

Rino S, Komiya T, Windley BF, Katayama I, Motoki A, Hirata T (2004) Major episodic increases of continental crustal growth determined from zircon ages of river sands; implications for mantle overturns in the Early Precambrian. Phys Earth Planet Inter 146(1–2):369–394

Saylor JE, Jordan JC, Sundell KE, Wang XM, Wang SQ, Deng T (2018) Topographic growth of the Jishi Shan and its impact on basin and hydrology evolution. NE Tibetan Plateau Basin Res 30:544–563

Shu P, Li B, Wang H, Qiu Y, Niu D, David D, An Z (2017) Geochemical characteristics of surface dune sand in the Mu Us Desert Inner Mongolia and implications for reconstructing the paleoenvironment. Quat Int 479:106–116

Stevens T, Palk C, Carter A, Lu H, Clift PD (2010) Assessing the provenance of loess and desert sediments in northern China using U-Pb dating and morphology of detrital zircons. Geol Soc of Am Bull 122(1):1331–1344

Stevens T, Carter A, Watson TP, Vermeesch P, Andò S, Bird AF, Lu H, Garzanti E, Cottam MA, Sevastjanova I (2013) Genetic linkage between the Yellow River the Mu Us desert and the Chinese loess plateau. Quat Sci Rev 78:355–368

Sun J (2000) Origin of eolian sand mobilization during the past 2300 years in the Mu Us desert China. Quat Res 53:78–88

Sun J (2002) Provenance of loess material and formation of loess deposits on the Chinese Loess Plateau. Earth Planet Sci Lett 203(3–4):845–859

Sun Y, Chen H, Tada R, Weiss D, Lin M, Toyoda S, Yan Y, Isozaki Y (2013) ESR signal intensity and crystallinity of quartz from Gobi and sandy deserts in East Asia and implication for tracing Asian dust provenance. Geochem Geophys Geosyst 14(8):2615–2627

Sun J, Ding Z, Xia X, Sun M, Windley BF (2018) Detrital zircon evidence for the ternary sources of the Chinese Loess Plateau. J Asian Earth Sci 155:21–34

Sun Y, Yan Y, Nie J, Li G, Shi Z, Qiang X, Chang H, An Z (2020) Source-to-sink fluctuations of Asian aeolian deposits since the late Oligocene. Earth-Sci Rev 200:102963

Sundell KE, Saylor JE (2017) Unmixing detrital geochronology age distributions. Geochem Geophys Geosyst 18(8):2872–2886

Vermeesch P (2004) How many grains are needed for a provenance study? Earth Planet Sci Lett 224(3–4):441–451

Vermeesch P (2012) On the visualisation of detrital age distributions. Chem Geol 312:190–194

Wan Y, Song B, Liu D, Wilde SA, Wu J, Shi Y, Yin X, Zhou H (2006) SHRIMP U-Pb zircon geochronology of Palaeoproterozoic metasedimentary rocks in the North China Craton: evidence for a major Late Palaeoproterozoic tectonothermal event. Precambrian Res 149(3–4):249–271

Wang Z, Wu Y, Tan L, Fu T, Wen Y, Li D (2019) Provenance studies of aeolian sand in Mu Us Desert based on heavy-mineral analysis. Aeolian Res 40:15–22

Wang P, Chen X, Zhu L, Xie H, Lv K, Wei X (2022) Principles and biases of quantitative provenance analysis using detrital zircon U-Pb geochronology: Insight from modern river sands. Acta Sedimentol Sin 40(6):1599–1614

Wiedenbeck M, AllÉ P, Corfu F, Griffin WL, Meier M, Oberli F, Von Quadt A, Roddick JC, Spiegel W (1995) Three natural zircon standards for U-Th-Pb, Lu-Hf, trace element and REE analyses. Geostand Newsl 4:335

Wu S, Pei X, Li Z, Li R, Pei L, Chen Y, Gao J, Liu C, Wei F, Wang Y (2012) A study of the material source of Dacaotan Group in the northern margin of West Qinling orogenic belt: LA-ICP-MS U-Th-Pb age evidence of detrital zircons. Geol Bull China 31(9):1470–1480

Xiao GQ, Zong KQ, Li GJ, Hu ZC, Dupont-Nivet G, Peng SZ, Zhang KX (2012) Spatial and glacial-interglacial variations in provenance of the Chinese Loess Plateau. Geophys Res Lett 39:L20715

Xie J, Wu F, Ding Z (2007) Detrital zircon composition of U-Pb ages and Hf isotope of the Hunshandake sandland and implication for its provenance. Acta Pet Sin 23(2):523–528

Xie J, Yang S, Ding Z (2012) Methods and application of using detrital zircons to trace the provenance of loess. Sci China-Earth Sci 55(11):1837–1846

Xiong JG, Wang Y, Picotti V, Zhang HP, Liu QR, Zhao XD, Su X, Zhang XL, Li YL, Zhang PZ (2023) Proximal supply in loess deposition of the Chinese loess plateau. JGR Earth Surf 128(3):814

Xu X, He S, Wang H, Zhang E, Chen J, Sun J (2008) Tectonic framework of North Qinling Mountain and North Qilian Mountain conjunction area in Early Paleozoic: a study of the evidences from strata and tectonic-magmatic events. Northwest Geol 41(1):1–21

Yang Y (2007) Study of driving factors of desertification in Mu Us Sandland. Dissertation, Northwest University

Yang S, Ding Z (2008) Advance-retreat history of the East-Asian summer monsoon rainfall belt over northern China during the last two glacialeinterglacial cycles. Earth and Planet Sci Lett 274:499–510

Yang W, Jolivet M, Dupont-Nivet G, Guo Z, Zhang Z, Wu C (2013) Source to sink relations between the Tian Shan and Junggar Basin (northwest China)

from Late Palaeozoic to Quaternary: evidence from detrital U-Pb zircon geochronology. Basin Res 25(2):219–240

Yang H, Zhang H, Luo B, Zhang J, Xiong Z, Guo L, Pan F (2015) Early Paleozoic intrusive rocks from the eastern Qilian orogen NE Tibetan Plateau: petrogenesis and tectonic significance. Lithos 224:13–31

Yang GL, Fan FX, Cai QS, Wang F, Zahng QS, Yan XY, Gao MM, Chen FH (2022) Provenance of Quaternary aeolian silts in western China and its spatial difference with source of the Yellow River sediments. Quat Sci Rev 296:107785

Yong Y, Xiao W, Yuan C, Yan Z, Li J (2008) Geochronology and geochemistry of Paleozoic granitic plutons from the eastern Central Qilian and their tectonic implications. Acta Petrol Sin 24:855–866

Zachos J, Pagani M, Sloan L, Thomas E, Billups K (2001) Trends rhythms and aberrations in global climate 65 Ma to present. Science 292(5517):686–693

Zhai M (2014) Multi-stage crustal growth and cratonization of the North China Craton. Geosci Front 5(4):457–469

Zhai M (2019) Tectonic evolution of the North China Craton. J Geomech 25(5):722–745

Zhai M, Peng P (2007) Paleoproterozoic events in the north China craton. Acta Petrol Sin 23(11):2665–2682

Zhang H, Lu H, Xu X, Liu X, Yang T, Stevens T, Bird A, Xu Z, Zhang T, Lei F, Feng H (2016) Quantitative estimation of the contribution of dust sources to Chinese loess using detrital zircon U-Pb age patterns. J Geophys Res: Earth Surf 121(11):2085–2099

Zhang HB, Nie JS, Liu XJ, Pullen A, Li GQ, Peng WB, Zhang HZ (2021) Spatially variable provenance of the Chinese Loess Plateau. Geology 49(10):1155–1159

Zhang H, Lu H, He J, Xie W, Wang H, Zhang H, Breecker D, Bird A, Stevens T, Nie J, Li G (2022) Large-number detrital zircon U-Pb ages reveal global cooling caused the formation of the Chinese Loess Plateau during Late Miocene. Sci Adv 8:eabq2007

Zhao G, Zhai M (2013) Lithotectonic elements of Precambrian basement in the North China Craton: review and tectonic implications. Gondwana Res 23(4):1207–1240

Zhu Z, Wu Z, Liu S, Di X (1980) An outline of Chinese deserts. Science Press, Beijing, pp 8–12

Zou N (2017) Distribution of U-Pb ages of the detrital zircon from the Hobq Desert and its implications for provenance. Dissertation, Northwest University

Publisher's Note